Est. 1984

ORIENTAL JOURNAL OF CHEMISTRY
An International Open Access, Peer Reviewed Research Journal

www.orientjchem.org

ISSN: 0970-020 X
CODEN: OJCHEG
2020, Vol. 36, No.(6):
Pg. 1049-1065

Transition Metals Ni^{2+}, Fe^{3+} Incorporated Modified ZnO Thick Film Sensors to Monitor the Environmental and Industrial Pollutant Gases

RAVINDRA HARIBHAU WAGHCHAURE[1,2]*, PRASHANT BHIMRAO KOLI[3], VISHNU ASHOK ADOLE[4], BAPU SONU JAGDALE[4] and THANSING BHAVSING PAWAR[1]

[1]Research Centre in Chemistry, Loknete Vyankatrao Hiray Arts, Science and Commerce College Panchavati, Nashik-422003, India

[2]Department of Chemistry, Mahant Jamanadas Maharaj Arts, Commerce and Science College, Karanjali, Taluka-Peth, District-Nashik-422 208, India.

[3]Department of Chemistry, Arts, Commerce and Science College, Nandgaon, Taluka-Nandgaon, District-Nashik-423106, India.

[4]Department of Chemistry, Arts, Science and Commerce College, Manmad, Taluka-Nandgaon, District-Nashik, India-423104.

*Corresponding author E-mail: waghchaureravindra86@gmail.com

http://dx.doi.org/10.13005/ojc/360607

(Received: October 30, 2020; Accepted: November 01, 2020)

ABSTRACT

Zinc oxide is known as multifaceted material due to its special physical and chemical properties. Present research deals with the fabrication of undoped ZnO, 1.5% Fe^{3+} doped ZnO, and 1.5% Ni^{2+} doped ZnO nanoparticles by low-cost co-precipitation method. These prepared materials were utilized to prepare thick film sensors by employing a screen printing technique. The structural confirmations of these materials were performed by various nano-characterization techniques. The structural properties were investigated by XRD to confirm the nanoscale ZnO as well as the average crystal dimensions. The surface morphological properties of undoped and modified ZnO were analyzed by SEM and TEM methods. The average volume pores over prepared materials and surface area were concluded from the N^2 adsorption-desorption experiment (BET analysis). The Fe^{3+} doped ZnO has the highest surface area among all the prepared sensors i.e. 23.55 m^2/g. The Fe^{3+} doped ZnO and Ni^{2+} ZnO nanomaterials were observed to show declined band gaps in comparison to the undoped ZnO material. All the prepared sensors were employed for the gas sensing study of gases like NH_3, LPG, formaldehyde vapors, toluene vapors, CO, CO_2, and NO_2. The CO_2 and NH_3 vapors found to be very sensitive towards Fe^{3+} doped ZnO with 76.62% and 76.58% sensitivity respectively. The Ni^{2+} doped ZnO sensor sensitivity for CO_2 and NH_3 was recorded as 71.20% and 70.23% respectively. The LPG, CH_2O, and toluene vapors' sensitivity was also studied for the modified ZnO sensor. Besides, modified ZnO utilized as a relative humidity sensor with an RH variation of 10-90%. The impedance versus humidity curves recorded for all sensors. The Fe^{3+} doped ZnO nanomaterial at 10 Hz was found to be an effective humidity sensor. The response and recovery were found to be very rapid in Fe^{3+} doped ZnO for NH_3, CO_2, NO_2, and LPG vapors.

Keywords: Modified ZnO sensor, CO_2, NO_2, NH_3 gas sensing, Humidity sensor, BET, TEM.

INTRODUCTION

Nanotechnology is a productive technology that has become standout in various scientific fields due to its wide range of applications[1-5]. Nanotechnology is diverse technology found to be very prominent in various fields of science and engineering technology. The amazing applications of nanomaterials are listed in various beneficial and scientific fields such as optoelectronics, gas sensing, batteries, solar cells, effluent treatment, organic synthesis and conversions, energy conversion, fuel technology, defense system, agriculture, medicinal, pharmaceutical sectors, biosensing, catalysis, water purification technology, adsorbent materials, electronics mechanical applications, etc.[6-26].

There is a huge increase in the pollution around the atmosphere due to increasing industrialization. There are plenty of side effects and health hazards due to the consumption of these toxic gases[27-30]. The environmental safety has become a prime important thing in recent times[31-33]. Many incidents have been reported regarding toxic gas leakage and their severe side effects[34]. Thus, toxic gases evolved by industries must be detected in their threshold limit value (TLV). Most of the reports have been issued about the detection of toxic vapors/gases by the use of various semiconducting bases sensors[35-37]. The semiconducting metal oxides (SMO) based sensors found to be very promising materials for the sensing purpose of various gases[38-40]. Although there are plenty of SMO based sensors that have been designed as gas sensors in the form of thick or thin films, the zinc oxide semiconducting sensor is the most intensively reported gas sensor for a wide range of gas sensing applications. There are many advantages for choosing ZnO based sensors such as low-cost synthesis methods, no toxicity, high thermal stability, excellent catalyst performance, porous nature, good surface area, reproducible results, etc. Many methods have been accounted for the synthesis of zinc oxide nanoparticles, such as co-precipitation, sol-gel, spray pyrolysis, chemical vapour deposition, mechanical, hydrothermal, ultra sonication, microwave techniques, etc.[41-48]. The properties like corrosion-resistivity, low electrical conductivity, antimicrobial activity, good heat resistance, mechanical stability, high catalytic activity, and its non-toxic nature make it unique amongst metal oxide nanoparticles.

Apart from sole semiconducting metal oxide as a sensing device, there are many new techniques by which a more useful sensing device could be designed. Nanocomposites, binary oxides, inner transition metal oxides (ITMO), CNT based sensors, graphene-based sensors, conducting polymers composites based sensors, C, N, S doped sensors, transition metal and non-metal doped sensors, and intrinsic conducting polymer-based sensors were used for the sensing purpose of a large variety of gases[49-59]. Moreover, the transition metal-doped oxides are found to be very useful to design a high-quality sensor. According to the literature, the d-block metals dopant could decrease the bandgap in semiconducting metal oxide like ZnO and enhance their optical properties[60-62]. Zinc oxide nanomaterial occurs in different types of structures. The one-dimensional form includes nanorods, needles, belts, wires, etc., two-dimensional form includes nanosheets and the three-dimensional form includes flowers, snowflakes, etc. The zinc oxide material can exist in three types of crystal lattice; wurtzite, zinc blende and rock salt. The thermodynamically most stable form is the wurtzite structure in which the zinc is co-ordinated with the four oxygen atoms in a tetrahedral shape. Most of the semiconducting metal oxides have bandgap in the range of 3.5-4 eV by using the metal dopants the bandgap is reduced for the semiconducting metal oxides[63,64]. In addition, many structural and electronic properties can be enhanced for most of the pure semiconducting materials[65,66]. Hence transition metal doping is effectively utilized to modify many structural and electronic properties of the undoped materials.

There are many hazardous gases that evolved during the chemical processes, due to the burning of fuels, chemical reactions, petroleum refining and automobile exhaust. These toxic gases are harmful to both the animals and plants. In many cases the severe breathing problems, respiratory infections, cyanosis, suffocation, dullness, skin and eyes irritation, and other severe damages to the environment and plants. In the present research, undoped and doped zinc oxide nanoparticles were prepared by the co-precipitation method and their thick films were prepared by the screen printing method. The prepared sensors were utilized to sense some of the hazardous gases such as CO, CO_2, NO_2, NH_3, LPG, formaldehyde vapors, toluene vapors, and also for relative humidity. The main purpose of

the doping transition metals into the ZnO lattice was to investigate comparative results between undoped ZnO and modified ZnO. The modified ZnO has porous nature, improved surface area and declined band gap, hence operated as highly efficient sensors for NH_3, CO_2, NO_2, LPG vapours and relative humidity.

MATERIALS AND METHODS

All the chemicals used in the synthesis are of AR grade purchased from a local distributor, Nashik (Make: Sigma-Aldrich and SD fine) and were used without further purification. Chemicals used are $Zn(NO_3)_2.6H_2O$,$Fe(NO)_3.9H_2O$,$Ni(NO_3)_2.6H_2O$, NaOH and deionized water.

Synthesis of Zinc oxide by co-precipitation method

ZnO nanoparticles were synthesized by the co-precipitation method using zinc nitrate ($Zn(NO_3)_2.6H_2O$) and NaOH as precursors. In the present method, an aqueous solution (0.02 M) of zinc nitrate was prepared with deionized water. This solution was stirred on a magnetic stirrer at room temperature for 30 minutes. After this, the solution was stirred at 80°C and 0.02 M NaOH was added dropwise over a period of 30 minutes until pH=12. After the complete addition of NaOH, the solution turns turbid and was stirred at 80°C further for 3 hours. Then it was subjected to ultrasound irradiation for a period of 30 minutes. The obtained off white product was centrifuged at 5000 rpm for 30 min and washed with deionized water and ethanol. The obtained product was dried at 110°C in an oven for 12 h and then grinded using mortar-pestle. The finely grinded product was then calcined at 500°C in a muffle furnace for 3 h to obtain zinc oxide nanoparticles.

Synthesis of Fe^{3+} doped zinc oxide and Ni^{2+} doped Zinc oxide nanomaterials

Similar method which was used for the synthesis of undoped ZnO is used for the synthesis of Fe^{3+} doped ZnO and Ni^{2+} doped ZnO materials. The 1.5% mole concentration doping was carried out for incorporating Fe^{3+} and Ni^{2+}.

Fabrication of thick film sensor of undoped ZnO nanoparticles

The thick film sensor of undoped ZnO nanomaterial was prepared by the screen printing method. Here the inorganic and organic proportion was sustaining 70:30 respectively. The inorganic part consists of undoped ZnO nanoparticles, while the organic segment consists of 8% BCA (Butyl Carbitol Acetate) and 92% ethyl cellulose. All these compounds weighed and diversified in mortar and pestle (clean and dried by acetone) for nearly 30 min To this mixture BCA was appended dropwise slowly to the above blend to obtain the psedoplastic phase (thixotropic), to get a viscous paste. This pulp was then applied on previously cut glass substrate (2x2 cm), by the screen printing procedure. The polymer film of nylon (40 s, mesh number 355) was utilized for the screen printing technique. The standard mask size was developed on the shade by the photolithography technique. After complete coating, the films were dried at atmospheric temperature for 20 min and then films were dried under an infra-red lamp for 30 minutes. Then these thick film sensors were calcined under muffle furnace at 450°C for 3 hours. The undoped ZnO thick film sensors are now ready for characterization and further use.

Fabrication of thick film sensor of 1.5% Fe^{3+} doped ZnO and 1.5% Ni^{2+} doped ZnO nanoparticles

The thick film sensors of 1.5% Fe^{3+} doped ZnO and 1.5% Ni^{2+} doped ZnO nanoparticles prepared by a standard screen printing method. Here the inorganic and organic proportion was sustaining 70:30 respectively. The inorganic part consists of 1.5% Fe^{3+} doped ZnO and 1.5% Ni^{2+} doped ZnO nanoparticle while the organic segment consists of 8% BCA (Butyl Carbitol Acetate) and 92% ethyl cellulose. All these compounds weighed and diversified in mortar and pestle (cleaned and dried by acetone) for nearly 30 min To this mixture BCA was appended dropwise slowly to the above blend to obtain the psedoplastic phase (Thixotropic), to get a viscous paste. This pulp was then applied on previously cutted glass substrate (2x2 cm), by screen printing procedure. The polymer film of nylon (40 s, mesh number 355) was utilized for the screen printing technique. The standard mask size was developed on the shade by the photolithography technique. After complete coating, the films were dried at atmospheric temperature for 20 min and then films were dried under infra-red lamp for 30 minutes. Then these thick film sensors were calcined under muffle furnace at 450°C for 3 hours. The undoped ZnO thick film sensors are now ready for characterization and further use.

Thickness measurement of the films

The surface coating of the films was measured by using equation (1), the thickness of the undoped ZnO films was found to be 7.407 um (7407 nm), for 1.5% Fe^{3+} doped ZnO, the thickness of the film was found to be 6.51µm (6510 nm), while thickness for 1.5% Ni^{2+} doped ZnO observed to be 6.213 µm (6213 nm). The thickness of all the prepared sensors was measured by mass difference method. The thickness of the film was found in the thick region.

$$t = \Delta M / A \times \rho \quad (1)$$

ΔM = Mass difference of the film before and after deposition

ρ = Composite density of undoped and doped zinc oxide (ZnO)

A= Area of the films

RESULTS AND DISCUSSION

X-ray diffraction (XRD) studies

The undoped ZnO, Fe^{3+} doped ZnO and Ni^{2+} ZnO calcined at 500 were characterized by XRD, with model number D8 advance Bruker AXS GmbH (Germany). The films were analyzed at Room temperature with CuKα radiations (wavelength 1.54 Å). The XRD spectrum as depicted in Fig. 1a-c shows the formation of crystalline zinc oxide as per data obtained. The Braggs reflection peaks are attributed to the formation of ZnO hexagonal lattice with crystal lattice and p63mc space group, having molecular weight 81.38 g/mole with a volume of lattice 47.62. The match scan data of ZnO shows the formation of crystalline ZnO nanoparticles with JCPDS number 00-036-1451. Diffraction peaks obtained are 31.79, 34.45, 36.28, 47.59, 56.66, 62.93, 68.02, 69.18, 72.66, 77.04 can be assigned to the reflection of (100), (002), (101), (102), (110), (103), (200), (112), (201), (202) planes. No additional peaks of any compound or impurity were observed in the XRD spectrum indicating that the prepared zinc oxide is pure. The diffraction peaks for Fe^{3+} doped ZnO and Ni^{2+} doped ZnO have nearly same two theta values in comparison to the undoped ZnO. Since the dopant concentration was not very sufficient to shift the two theta values largely. All the above-cited diffraction patterns confirm the formation of ZnO nanoparticles. The average particle size was calculated by using Debye-Scherer's formula. [$D = K\lambda/\beta \cos\theta$], where D is average particle size, K is constant (0.9 to 1), β is full-width half maxima (FWHM) of the diffracted peak, θ is the angle of diffraction. The average particle size for undoped zinc oxide was found to be 23 nm, for 1.5% doped Fe^{3+} it was 19 nm and for 1.5% Ni^{2+} doped ZnO, it is found to 29 nm.

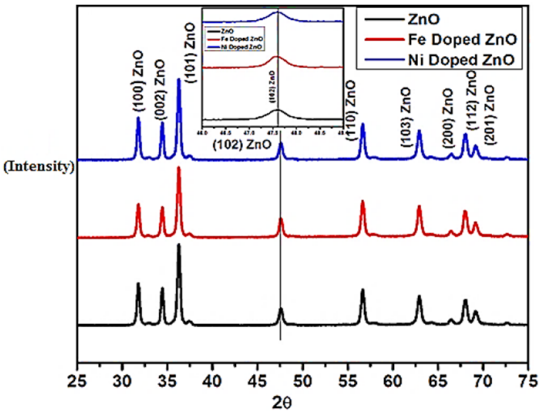

Fig. 1 (a). XRD spectrum of undoped ZnO thick films (b) XRD spectrum of 1.5% Fe^{3+} doped ZnO thick films. (c) XRD spectrum of 1.5% Ni^{2+} doped ZnO thick films

Field Emission Gun Scanning Electron Microscopy: (FEG-SEM)

The surface morphology, surface and porosity of the ZnO nano powder was affirmed from scanning electron microscopy. Fig. 2 a-f shows the SEM micrographs of undoped ZnO, 1.5% Fe^{3+}'doped ZnO and 1.5% Ni^{2+} doped ZnO nanoparticles respectively. The undoped ZnO is given in Fig. 2 a-c distinctly appearing with a hexagonal crystal lattice with heterogeneous structure alongside some void space over the cross section. The 1.5 % doped Fe^{3+} ZnO nanoparticles images as depicted in Fig. 2-b where the large voids/cavities are seen alongside the crystal lattice of ZnO. The 1.5% Ni^{2+} doped ZnO images are given in Fig. 2-c. Here the flakes crystals of ZnO appeared in hexagonal shaped can be seen with the various dimensions. From the SEM pictures, it can be seen that the undoped and doped ZnO are exceptionally permeable with certain voids over the outside of the cross section. Normal permeable material is exceptionally valuable for the detecting component, as the permeable material gives straightforwardness to adsorb the gases/vapors yielding the more reaction for vaporous particle superficially through chemisorption and physisorption. In doped ZnO framing littler chunks of different nanosized nanoparticles, while in undoped ZnO the little estimated nanoparticles are exceptionally

agglomerated to shape a heterogeneous cross section can be seen from SEM pictures. Overall, SEM images of all materials indicate that prepared materials have a good surface nature. All the gas sensing properties are surface properties, hence the interstitial voids present all over the surface of undoped and doped ZnO found to be effective for gas sensing phenomenon.

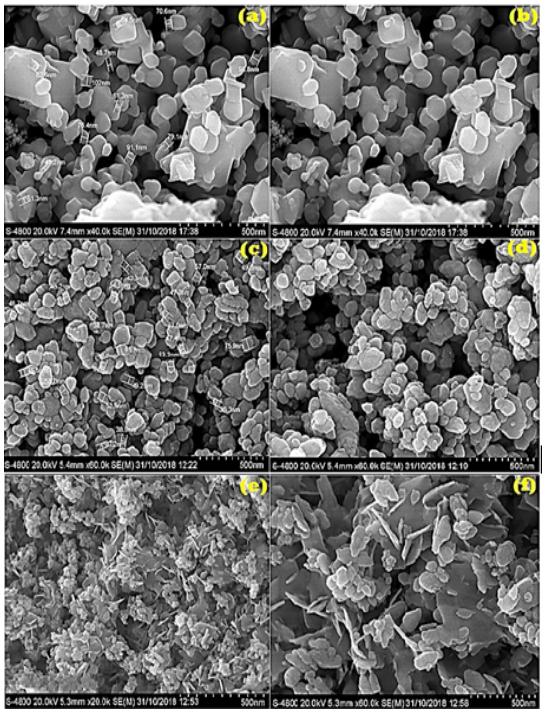

Fig. 2 (a-b). SEM image of undoped ZnO (c-d) SEM image of 1.5% Fe^{3+} doped ZnO (e-f) SEM image of 1.5% Ni^{2+} doped ZnO

Energy dispersive spectroscopy (EDS)

The energy dispersive spectroscopy was utilized to investigate the elemental composition of prepared material ZnO, Fe^{3+} doped ZnO and Ni^{2+} doped ZnO. All prepared material is found in proper elemental composition as represented in Fig. 3 a-c. In the EDS spectrum the elements have appeared in their normal scale position. For instance, in all the EDS spectrum represented in Fig. 3 a-c the elemental zinc is resolute at 8.5 KeV. The iron is resoluted at characteristic scale of 8.5 KeV and nickel is sharply resolved at 7.5 KeV scale. The elemental oxygen is resoluted at characteristic scale of 1.0 KeV in a very spectrum of undoped and doped ZnO depicted in Fig. 3 a-c. Thus, the prepared materials undoped ZnO and doped ZnO are in proper elemental and weight composition. The composition of all these elements is tabulated in their EDS spectrum.

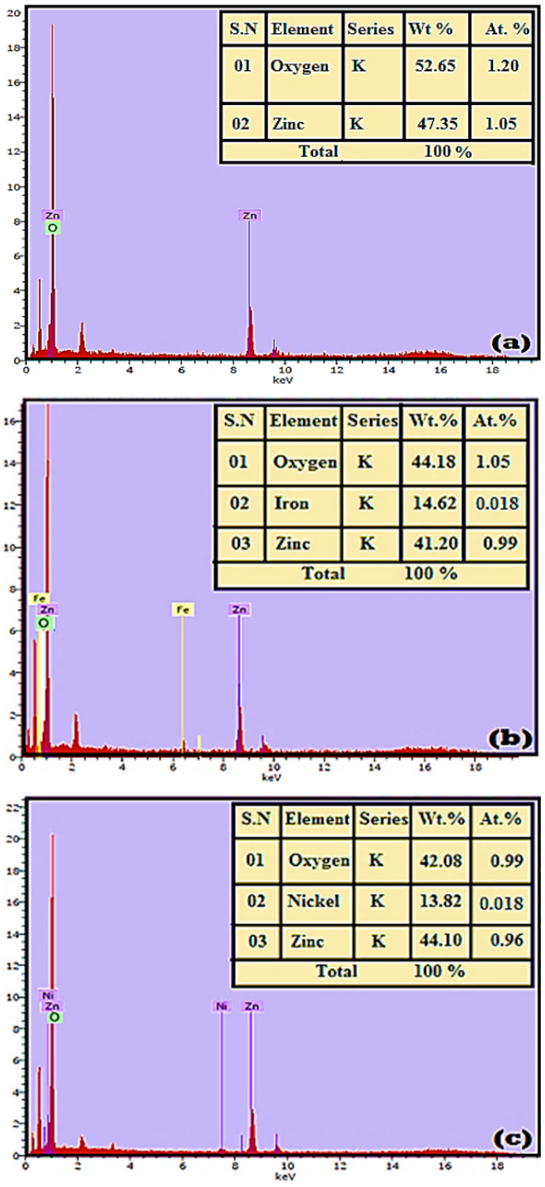

Fig. 3 (a). EDS spectrum of undoped ZnO (b) EDS spectrum of 1.5% Fe^{3+} doped ZnO (c) EDS spectrum of 1.5% Ni^{2+} doped ZnO

Brunauer-Emmett-Teller (BET)

Brunauer-Emmett-Teller (BET) analysis was performed for undoped ZnO, Fe^{3+} doped ZnO and Ni^{2+} doped ZnO thick film sensors with the ease of nitrogen adsorption-desorption experiment. This experiment was utilized to seek the information of porous material, as well as pore size distribution over the catalyst/sensor surface since, all the sensors were utilized for the gas sensing phenomenon which is a surface property. Hence,

the investigation of the available surface area for chemisorption or physisorption among adsorbate gas molecules and adsorbent sensors is a prime investigation for the gas sensing study. The data obtained from BET analysis i.e. surface area, pore volume/radius, pore size etc. is represented in Table 1. On the other hand, the BET analysis via nitrogen adsorption-desorption experiment is represented in Fig. 4 a-c. Among the six BET standard adsorption isotherm, the present isotherm represented in Fig. 4 belongs to type –IV adsorption isotherm from BDDT system for BET analysis.

Table 1: BET N_2 adsorption-desorption curves for undoped ZnO, 1.5% Fe^{3+} doped ZnO 1.5% Ni^{2+} doped ZnO

Prepared Material	Surface Area (m^2/g)	Pore volume (cc/g)	Pore radius (Å)	R2
Undoped ZnO	13.538	0.0380	104.71	0.9998
1.5% Fe^{3+} doped ZnO	23.552	0.0870	107.39	0.9998
1.5% Ni^{2+} doped ZnO	16.134	0.0316	104.68	0.9997

High-resolution transmission electron microscopy (HR-TEM)

The crystal lattice of the modified ZnO material was investigated by means of high-resolution transmission electron microscopy as depicted in Fig. 5 a-c with the resolution at 10 nm, 20 nm and 50 nm respectively. Similarly, the image appeared in Fig. 5d represents selected area diffraction pattern for the modified ZnO material. These bright spots can be assigned to the (h, k, l) planes of prepared material for the characteristic of prepared material. The bright spots that appeared in the SAED pattern constitute the crystalline nature of prepared material. Data obtained for 1.5% doped ZnO material implies formation hexagonal crystal lattice. The images a-c in Fig. 5 justifies the prepared ZnO material with nearly hexagonal type lattice matches with reported literature. As well the TEM results obtained for the prepared material are found to be in good agreement with XRD data. Since X-ray diffraction data for the all prepared sensors proclaims the formation hexagonal crystal lattice.

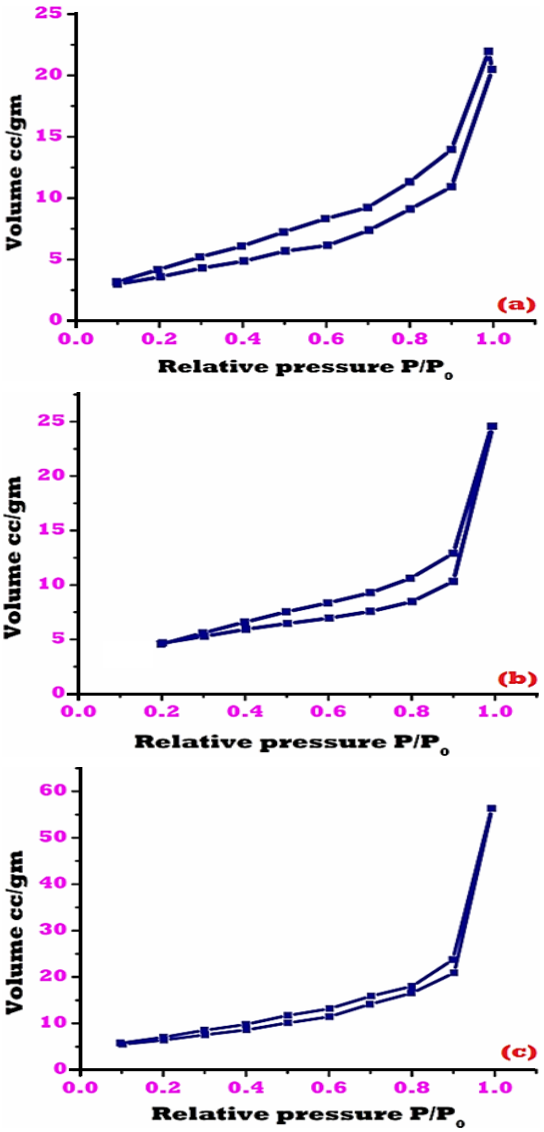

Fig. 4. N_2 adsorption-desorption curves for (a) undoped ZnO, b) 1.5% Fe^{3+}, doped ZnO (c) 1.5% Ni^{2+} doped ZnO

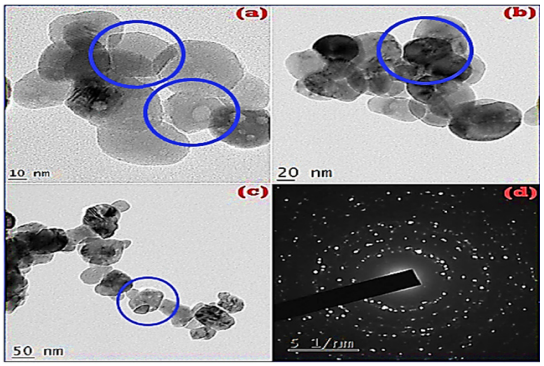

Fig. 5 (a-c). HR-TEM images of 1.5% Fe^{3+} doped ZnO sensor (d) SAED pattern for 1.5% Fe^{3+} doped ZnO sensor material

Electrical resistivity and temperature effect on undoped ZnO, 1.5% Fe^{3+}, doped ZnO and 1.5% Ni^{2+} doped ZnO sensors

The electrical resistivity and consequence of elevated temperature on screen-printed thick film sensors of undoped ZnO, Fe^{3+} doped ZnO and Ni^{2+} doped ZnO were investigated to conclude about the semiconducting behavior of the sensors. The electrical characteristics and gas sensing properties of thick film sensors were investigated with regular potential divider experimental arrangements. Thick film sensors were mounted at the base of the gas assembly chamber in the sample section. In this section Cr-Al thermocouple fixed with the sensor cavity to sense the temperature across the sensors plates. The change in temperature was accessed digitally by temperature recorder with model number PEW-202/PEW-205 from a thermocouple attached to the sensor. The temperature was supplied across the film from 400°C to 50°C. The electrical resistance of all the films was measured in the existence of oxygen and without interruption of any other gases in the glass-domed shaped chamber with the regular set up as depicted in Figure 6.

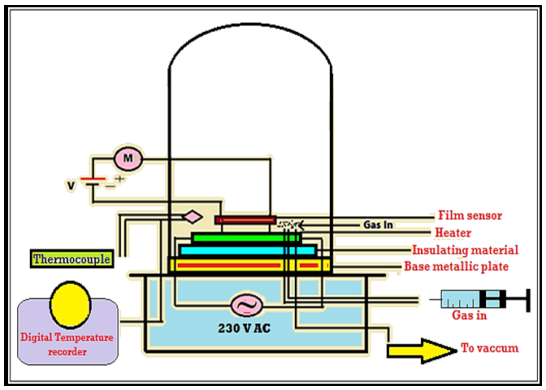

Fig. 6. Gas sensing model diagram utilized in present research

The effect of temperature on the prepared sensors can be seen in Fig. 7. (a,c,e) here the resistance of the film sensor found to be very high at the commencing stage, but with an increment of temperature from 50°C to 400°C, the resistance found to be decreased steadily. The declined resistance is a result of expanding stream versatility of the charge moving or because of grid vibrations related to developing temperature. Where the molecules frequently approach adequate for the exchange the rate transporters and the conduction is started with the guide of cross-section vibration as shown in Fig. 7 a-c. The effect of temperature and activation energy of the prepared thick film sensors was calculated using equation 2 from the plot of Log R versus 1/T as shown in Fig. 7 (b, d, f). During the effect of temperature on the prepared sensors, the cumulated resistivity exhibited by the sensors is an important parameter to conclude about the electrical behavior of the sensors. The total resistivity calculated by equation 3.

$$R = R0\ e^{-\Delta E/KT} \quad (2)$$

R = Resistance varied at different temperatures, R_0 = Resistance at 0°C, $\Delta E/T$ = Variation of energy with temperature i.e. activation energy, ΔE = 2.303 *K* Slope (Calculated from graph), K= Boltzmann Constant (8.61733 X 10^{-5} $eV.K^{-1}$).

$$\rho = R.b.t/L \quad (3)$$

ρ = Resistivity of the film, R = resistance at room temperature, b = breadth of film, t = thickness of the film, L = length of the film.

LT = Low temperature , HT= High temperature

Gas sensing study of prepared sensors for selected gases

The gas sensing study for prepared thick film sensors was performed for some selected gases such as CO, CO_2, NO_2, NH_3, LPG, formaldehyde vapors and toluene vapors (TV). The entire gas sensing experiment was performed by using the homemade gas sensing assembly set up as depicted in Fig. 6. The resistance of the thick film sensors was measured by using the half-bridge method. Here altering the resistance of the thick film sensor resulted in a change in voltage over definite resistance. The voltage over definite resistance, the particular resistance of the film is inter-convertible and can be calculated easily with the aid of Ohms law. The desired concentration of gas was introduced inside the gas chamber and the fixed DC voltage was applied to the film circuit. The film sensor resistance was monitored by digital output voltage millimetre with model number CIE Classic 5170. Every time the selected gas allowed introducing inside the dome-shaped glass chamber, the output voltage response between sensor circuit and gas was recorded with a millimetre. The gas residue was cleaned by supplied fixed temperature inside the gas sensing assembly through the thermostat. The electrical resistance of thick film sensor in the existence of air (Ra) and presence of gas (Rg) was measured to estimate the % response or sensitivity by the sensor to tested gas, given by equation 4.

$$S\% = Ra\text{-}Rg/Ra*100 \quad (4)$$

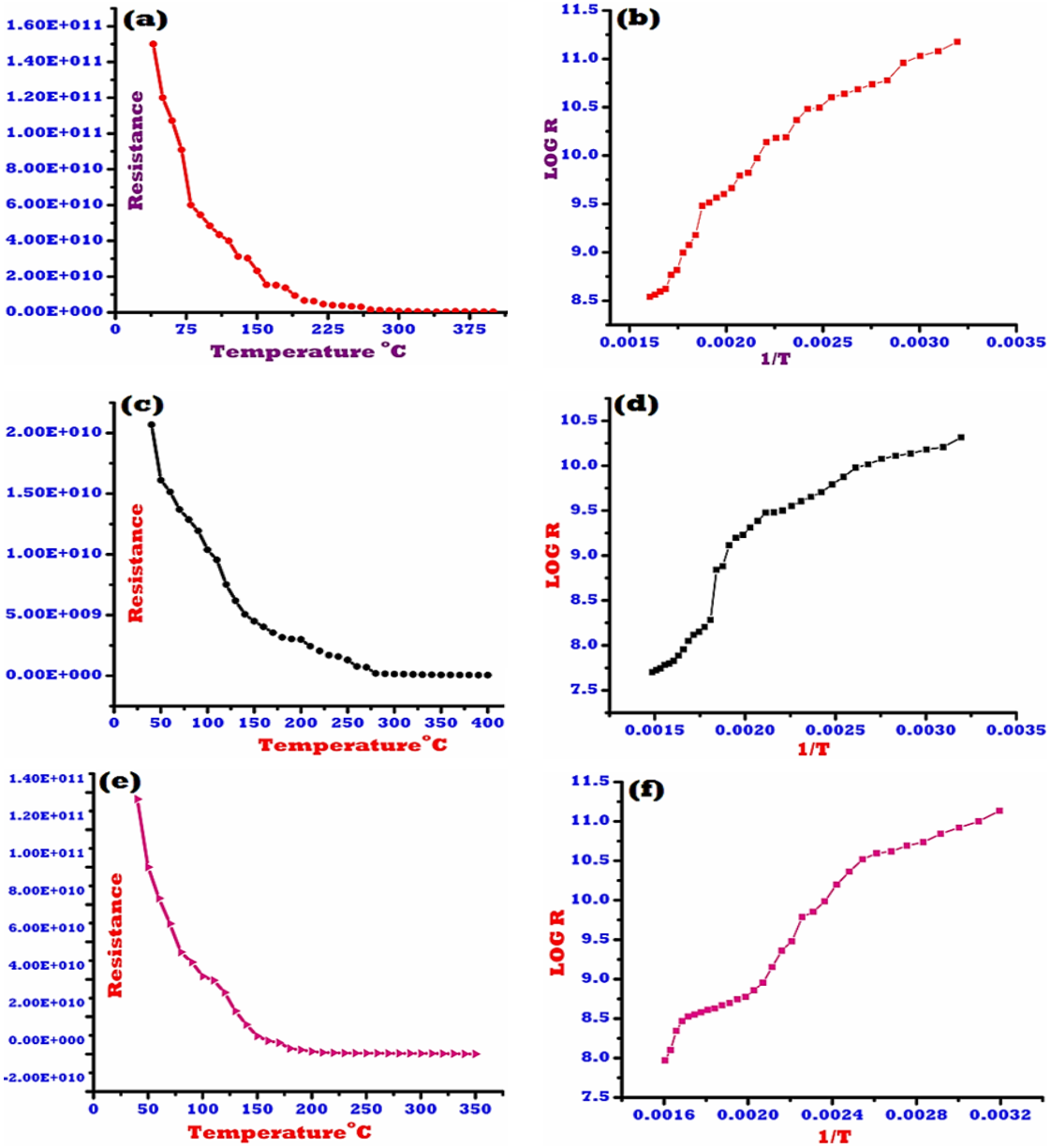

Fig. 7 (a). Variation of resistance with temperature for undoped ZnO (b) plot of 1/T versus log R for activation energy undoped ZnO (c) variation of resistance with temperature for 1.5% Fe^{3+} doped ZnO (d) plot of 1/T versus log R for activation energy 1.5% Fe^{3+} doped ZnO (e) variation of resistance with temperature for 1.5% Ni^{2+} doped ZnO (f) plot of 1/T versus log R for activation energy 1.5% Ni^{2+} doped ZnO

Table 2: Resistivity, activation energy and average grain size for undoped ZnO, 1.5% Fe^{3+} doped ZnO and 1.5% Ni^{2+} doped ZnO sensors

Thick film sensor	Grain Size From XRD (nm)	Resistivity (Ω m)	Activation Energy (eV)	
			L.T.	H.T.
Undoped ZnO	23	11.032×10^5	0.1674	0.2717
1.5% Fe^{3+} doped ZnO	19	6.265×10^3	0.1939	0.2513
1.5% Ni^{2+} doped ZnO	29	7.144×10^3	0.1825	0.232

Gas sensing and electronic characteristics of prepared sensors

ZnO is widely used in semiconducting sensor material for a large category of gases. The estimated band gap range of ZnO is 3.4 eV and it shows typical n-type semiconducting behavior. The n-type semi conduction is attributed to native defects or oxygen vacancies. The inherent carrier density of zinc oxide is found to be 106/cm^{-3} at a normal temperature. While it's internal donor level is nearly 0.5-0.15 eV beneath the conduction band. According to reports its donation density at room temperature is approximately 10 17 /cm^{-3}. The positive hole movement capacity is 5-50 cm^2/(Vs), while the negative ion (electrons) mobility is 200 cm^2/cm^{-3}. All these electronic parameters make ZnO an excellent sensor to sense the wide category of gases. Here tripositive Fe and dispositive nickel is doped into the ZnO lattice. Due to the Fe^{3+} doping NTC (negative temperature coefficient), the character of ZnO is altered to PTC (positive temperature coefficient) since the tripositive iron impurity/dopant providing the additional holes for the conduction. While in the case of nickel doped zinc oxide, some of the Zn^{2+} ions may be replaced by the Ni^{2+} dopant concentration but its NTC character remains to conserve.

Sensitivity of undoped ZnO and modified ZnO for selected gases

The most important parameter of a particular gas sensor is the response given by the sensor to the selected or tested gas so that it can be designed for commercial purposes to get used at demanding places. Here for gas sensing study some of the selected environmental and industrial toxic gases were selected that are exhausted in various chemical processes. The gases like CO, CO_2, NO_2, NH_3, LPG, formaldehyde vapors, and toluene vapors are toxic and selected for sensing purposes for the fabricated sensors in the present study. The optimum response recorded for these gases at different temperatures is listed in Table 3. The plot of % sensitivity against temperature is depicted in Fig. 8a-c. Undoped ZnO is popularly used as a promising sensor for many common gases such as H_2S, NH_3, Methane, SO_2, NO_2, Cl_2, acetone, ethanol, methanol, etc. Here we utilized the ZnO and modified ZnO to sense some highly toxic gas vapors like CO, CO_2, NO_2, NH_3, LPG, Formaldehyde vapors and toluene vapors (TV). Out of these above-listed gases very rare reports have reported on gas sensing properties of LPG, formaldehyde vapors, and toluene vapors (TV). Here very interesting results have been investigated for these toxic gases and especially Fe^{3+} doped ZnO was found to be very sensitive for these gases. The detailed statistics about the gas sensing study are highlighted in Table 3. The most interesting results obtained for Fe^{3+}/ZnO thick film sensor, here the response for the iron modified ZnO sensor for CO_2 to be 76.62% at 150°C and for NH_3 vapors response up to 76.58% at 150°C was observed for Fe^{3+}/ZnO thick film sensor. Similarly for CO, LPG, NO_2, CH_2O, toluene vapors, the response by Fe^{3+} doped ZnO was found to be 68.59%, 65.12%, 70.12%, 35.12% and 22.46% respectively. The interesting results for iron-doped ZnO are attributed to high surface area from BET analysis, declined bandgap of iron-doped ZnO in comparison to undoped ZnO, excellent porous nature of Fe^{3+}/ZnO thick film sensor which leads to highly efficient interaction between gases and surface-active sensor. The reduced bandgap in case of iron-doped ZnO, the conduction band of iron is close to the valence band of ZnO and hence the ease of electron transportation and redox mechanism is very rapid in case of iron-doped ZnO sensor surface amid the selected gases.

Table 3: Comparative chart for gas response in undoped ZnO, 1.5% Fe^{3+}doepd ZnO and 1.5% Ni^{2+}doepd ZnO at 100 ppm

Gas (100 ppm)	%S undoped ZnO	Optimum sensing Temperature (°C) undoped ZnO	%S Fe^{3+} doped ZnO	Optimum sensing Temperature (°C) Fe^{3+}doped ZnO	%S Ni^{2+} doped ZnO	Optimum sensing Temperature (°C) Ni^{2+}doped ZnO
CO	52.25	250	68.59	200	62.12	200
CO_2	55.12	100	76.62	150	71.2	150
NO_2	58.16	100	70.12	100	69.48	100
NH_3	59.23	150	76.58	150	70.23	150
LPG	62.15	100	65.12	100	63.12	200
CH_2O vapours	37.89	200	35.12	100	32.25	150
Toluene Vapours	19.58	100	22.46	200	20.12	100

TV = Toluene vapours, CH_2O = Formaldehyde, %S = Gas response, LPG = Liquefied petroleum gas

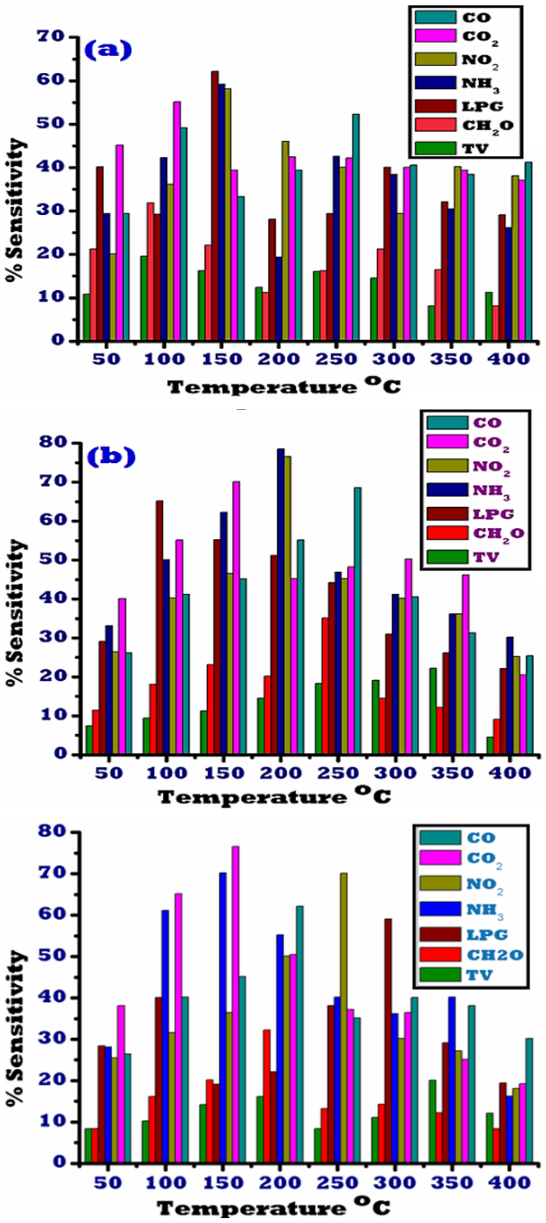

Fig. 8 (a). %sensitivity of tested gases at optimum temperature for undoped ZnO, (b) %sensitivity of tested gases at optimum temperature for Fe^{3+} doped ZnO, (c) %sensitivity of tested gases at optimum temperature for Ni^{2+} doped ZnO

Selectivity of undoped ZnO and modified ZnO for selected gases

The selectivity by the sensor to particular gas is a prime parameter for the every sensor material. In Fig. 9, the selectivity of all tested gases for fabricated thick film sensors is depicted. The selectivity of gases was computed by utilizing equation 5. From the data of calculation maximum selectivity was shown by bromine vapors. The prepared sensors viz. Fe^{3+} doped ZnO and Ni^{2+} doped ZnO sensors showed selectivity 100 % for CO_2 gas, and undoped ZnO showed 100% selectivity for LPG gas. The high selective gas after CO_2 observed to be ammonia vapors, showed sensitivity for undoped ZnO was 95.30%, then Fe^{3+} doepd ZnO at 99.94% and for Ni^{2+} doped ZnO showed selectivity for phosphine gas was 98.63%. The selectivity by other toxic gases was CO, NO_2, LPG, formaldehyde vapors and toluene vapors were also very high all the sensors. Previously the selectivity and sensitivity of toluene vapors, LPG, and formaldehyde vapors are very rarely reported for undoped and modified ZnO sensors. Percentage selectivity of all tested gases for prepared sensors is as depicted in Table 4.

$$\%Selectivity = (S_{target\ gas}/S_{High\ responding\ gas})*100 \quad (5)$$

$S_{other\ gas}$ – sensitivity of films for target gas

$S_{target\ gas}$- sensitivity for films for high responding gas

Table 4: Selectivity of prepared sensors for tested gases

Tested gases	%Selectivity for thick film sensors		
	Undoped ZnO	Fe^{3+}doped ZnO	Ni^{2+}doped ZnO
CO_2	88.68	100	100
CO	84.07	89.51	87.24
NO_2	93.58	91.51	97.58
NH_3	95.30	99.94	98.63
LPG	100	84.99	88.65
CH_2O vapours	60.96	45.83	45.29
TV	31.50	29.31	28.25

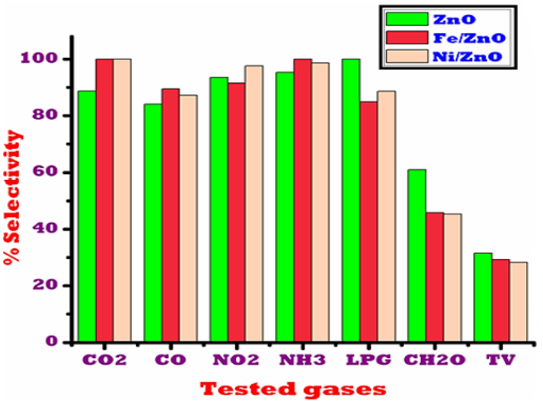

Fig. 9. Selectivity for tested gases by undoped ZnO and modified ZnO sensors

Humidity sensing performance of undoped and modified ZnO sensors

In most of the important fields like the medicinal sector, food processing units, research and development laboratories, clinical trials, etc. relative humidity (RH) plays a vital role in

maintaining good environmental conditions. Here prepared sensors utilized as humidity sensors in addition to gas sensors. There various types of humidity sensors, but ceramic types of sensors have an advantage due to small size, low-cost fabrication and high stability. The elevated signal arises in ceramic category sensors mainly due to the adsorption of aqua molecules nearby in the atmosphere or on the exterior of the sensing device. The change in output electrical signal against the relative humidity % is as shown in Fig. 10. It can be seen from Fig. 10 the change in output electrical signal for relative humidity is showing considerable variation for prepared sensor Fe^{3+} doped ZnO at different operational frequencies like 10 Hz, 100 Hz 500 Hz. The signal sharply changes for iron-doped ZnO sensors for 10 to 90% relative humidity at 10 Hz. It can be seen from Fig. 10 impedance rapidly declined more than three proportions when the relative humidity fluctuated from 10 to 90% exhibits the highest response and best regression throughout the humidity scale. Therefore 10 Hz is the optimum operational range in this setup. The change in resistance against relative humidity is as shown in Fig. 11. The highest response for iron-doped ZnO is can be seen from Figure 11.

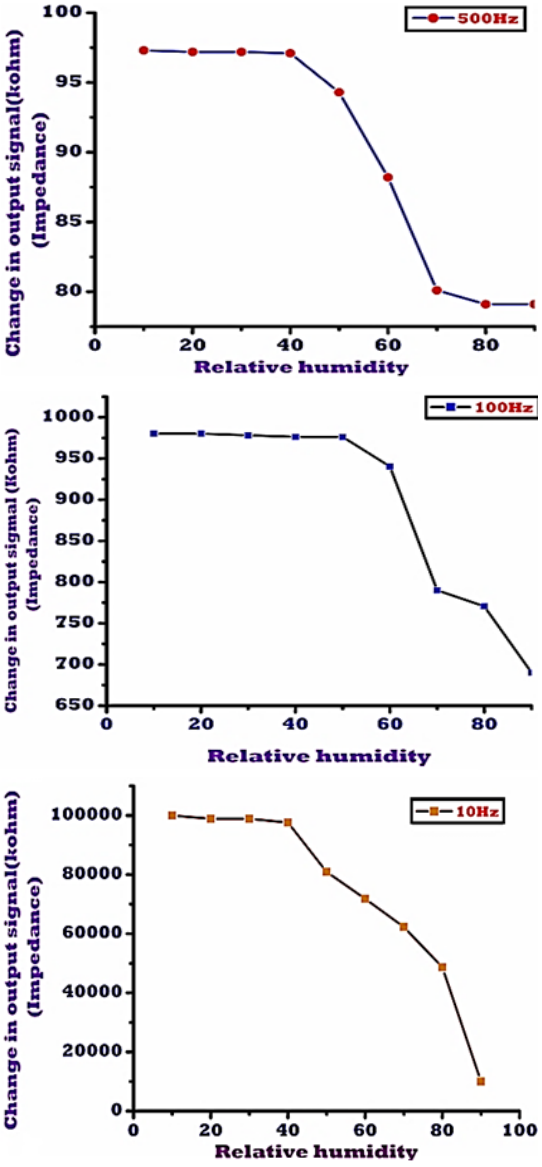

Fig. 10. Impedance verses relative humidity for prepared Fe^{3+} doped ZnO sensors at 10Hz

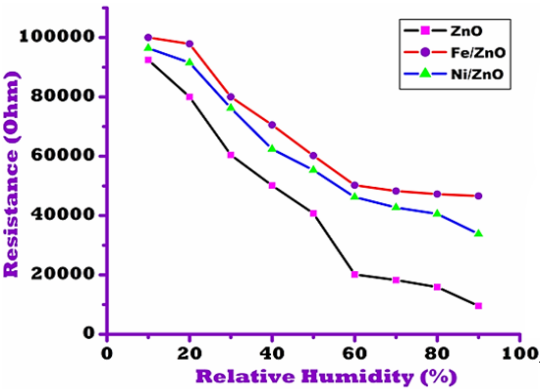

Fig. 11. The humidity loops characteristic of prepared sensor measured at 10 Hz

Response and Recovery

The response and recovery is an important parameter to design the sensor for a particular gas. In the present research best response was recorded for 1.5% Fe^{3+} ZnO sensor for bromine vapors, formaldehyde, ammonia, and toluene vapors. Hence response and recovery were conducted these four gases. For all these gases the response was recorded at 100 ppm gas concentration of each gas. The optimum response and recovery time for all the gases areas are mentioned in Table 5. As mentioned, the response and recovery rate was rapid for formaldehyde vapors and toluene vapors.

Table 5: Summary of response and recovery of tested gases for 1.5 % Fe^{3+} doped ZnO sensor

Entry	Gas	Response%	Response time in seconds	Recovery time in seconds
1	CO_2	76.62	33	54
2	NO_2	70.12	30	43
3	NH_3	76.58	22	45
4	LPG	65.12	18	38

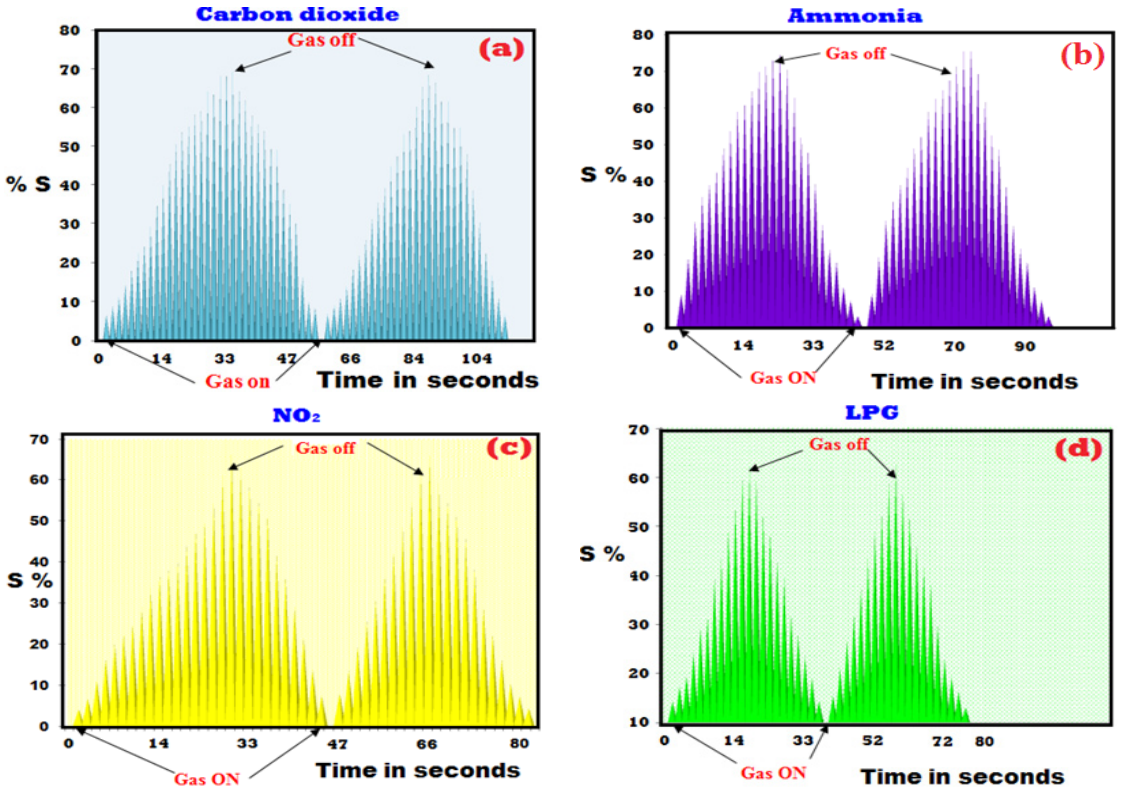

Fig. 12. Response and recovery graphs of 1.5% Fe^{3+} doped sensor for (a) Br_2, (b) formaldehyde vapours (c) ammonia vapours (d) toluene vapours

Recycling ability of prepared sensors

The recycling performance of ZnO, 1.5% Fe^{3+} ZnO, and 1.5% Ni^{2+} ZnO sensors was tested for bromine vapors; formaldehyde, ammonia, and toluene vapor sensors. The recycling performance is one of the prime parameters for the sensor. For the productive functioning of the sensor, the response for particular gas must be reproducible. Hence recycling performance of the gases was investigated. All the gases were operated at 100 ppm concentration and all sensors were tested periodically at the time interval of 8 days for the selected gases. The graphs representing the recycling performance of tested gases are represented in Fig. 13. After the repetition of every cycle for each gas, the percent response for each gas found declined with low variation. The observation concerning decrease in the response for each cycle after 8 days performance, the clarification could be give out to this decline is the lessening in the surface activity of the sensors. As these sensors oppressed as often as possible for the testing, the upper surface movement found to bring down due to uncovering of gas each time consequently its adsorption property brought down. In this manner, consistent abatement saw in the affectability reaction by these sensors.

Comparison of prepared sensors

The prepared modified (Fe^{3+} doped ZnO) ZnO thick film sensor prepared by the screen printing method was compared with other zinc nanocomposites, transition metal-doped ZnO sensors and ZnO based reported gas sensors and also other sensors. The iron modified ZnO catalyst used to sense the above-listed gas vapors and these modified sensors is found to be extraordinary for sensing these gases. In the present investigation modified ZnO catalyst is characterized by several properties. From this investigation, it is found that this catalyst has a considerable surface area and declined band in comparison to the undoped ZnO. Hence these modifications in structural and electronic properties construct the modified ZnO sensor different among the rest of the sensors to sense selected gases. The comparison of the tested gases for modified ZnO sensor and other reported ZnO based sensors is presented in Table 6.

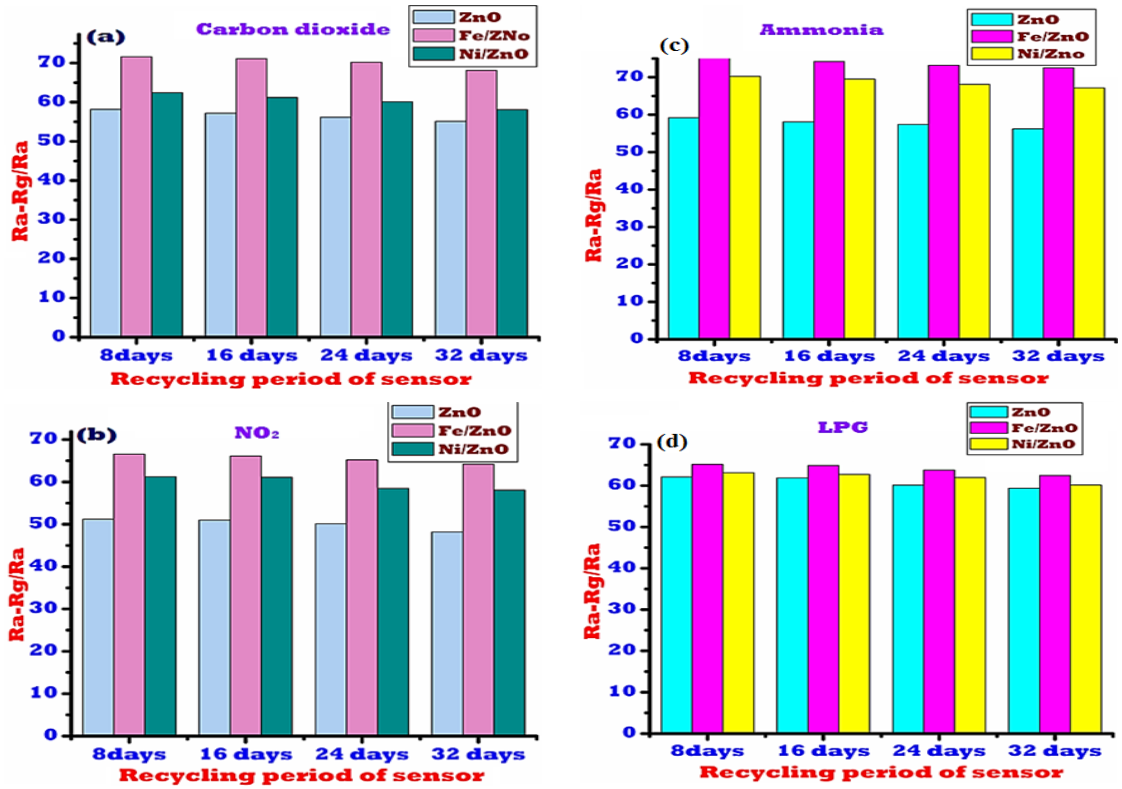

Fig. 13. Recycling performances of prepared sensors for (a) CO_2 (b) NO_2 (c) NH_3 (d) LPG

Table 6: Comparative studies of carbon dioxide for modified ZnO sensor and reported sensors

Sensor	Method of Fabrication	Type of sensor	Sensing Temp. (°C)	Gas in ppm (CO_2)	Reported Sensitivity (%)	Reference
CuO	Cinterred ceramics	Thin Film	250	5000	48	67
Fe_2O_3	Spin coating	Thin film	-	20	20	68
La_2O_3/SnO_2	LPCVD	Thin film	350	1000	30	69
$LaOC_3$	NW Coating	Thin film	400	4000	5	70
Cr^{3+},Co^{2+} doped $LaFeO_3$	Spin coating	Thin film	100	500	50.17	8
MoO_3:NiO	Hydrothermal	Thick film	150	1000	87.7	71
SnO_2-NiO/ZnO	RF-Sputtering	Thin film	-	--	-	72
1.5% Fe^{3+} doped ZnO	Screen printing	Thick film	150	100	76.62	Present work

CONCLUSION

The undoped ZnO, 1.5% Fe^{3+} doped ZnO, and 1.5% Ni^{2+} doped ZnO were prepared by the co-precipitation method, while thick films were fabricated with assists of standard screen-printed technique. These all sensors utilized for sensing of CO, CO_2, NO_2, NH_3, LPG, formaldehyde vapors, and toluene vapor. The ZnO and modified ZnO very rarely utilized for sensing purposes of CO_2, NH_3, NO_2 and LPG vapors. Among all three prepared sensors the Fe^{3+} doped ZnO sensor was found to be highly sensitive and selective for CO_2, NH_3, NO_2 and LPG vapors, approximately 76.62%, 76.58%, 70.12 %, and 65.12 response was recorded at 150°C, 150°C, 100°C, 100°C respectively for each as 100 ppm. The Fe^{3+} doped ZnO sensors were also utilized as a humidity sensor and high humidity sense was recorded in comparison to the undoped ZnO and Ni^{2+} doped ZnO sensor. The high gas sensing performance of the Fe^{3+} doped ZnO sensor may be attributed to the high surface area, porous nature, and reduced band gap. In the additional study, all three sensors have excellent recycling performance for CO_2, NO_2, NH_3, and LPG gases. The iron modified ZnO sensor has

rapid response and recovery for CO_2, NO_2, NH_3, and LPG gases. Thus, in comparison, it can be concluded the iron-doped ZnO sensor found to be exceptional sensor CO_2, NO_2, NH_3 and LPG gases at moderate temperature as well a good sensor for relative humidity.

ACKNOWLEDGMENT

Authors gratefully acknowledge central instrumentation facility, Savitribai Phule Pune University, Pune and Kavayitri Bahinabai Chaudhari North Maharashtra University, Jalgaon for characterization of samples. Authors also would like to thank Lokenete Vyankatrao Hiray Arts, Science and Commerce College Panchavati, Nashik (India) and Mahant Jamnadas Maharaj Arts, Commerce and Science College Karanjali, Peth (India), Department of Chemistry, Arts, Science and Commerce College, Manmad, District-Nashik, and Department of Chemistry, Arts, Commerce and Science College, Nandgaon, District-Nashik for providing necessary research facilities.

Conflict of Interest

The authors declare no conflict of interest.

REFERENCES

1. Qu, X., Alvarez, P.J. Li, Q.: *Applications of nanotechnology in water and wastewater treatment. Water Res.*, **2013**, 47, 3931-3946
2. Hussein, A. K.: Applications of nanotechnology to improve the performance of solar collectors–Recent advances and overview. *Renewable Sustainable Energy Rev.*, **2016**, *62*, 767-792
3. Saeedi, M., Eslamifar, M., Khezri, K. Dizaj, S.M.: Applications of nanotechnology in drug delivery to the central nervous system. *Biomed. Pharmacother.*, **2019**, *111*, 666-675.
4. Hussein, A. K.: Applications of nanotechnology in renewable energies-A comprehensive overview and understanding. *Renewable Sustainable Energy Rev.*, **2015**, *42*, 460-476.
5. Singh, E., Joshi, N. D., Sasode, S., Chouhan, N.: *Application of Nanotechnology in Agriculture. Biotica Research Today.*, **2020**, *2*, 163-165.
6. Wang, X., Summers, C. J., Wang, Z. L.: Large-scale hexagonal-patterned growth of aligned ZnO nanorods for nano-optoelectronics and nanosensor arrays. *Nano Lett.*, **2004**, *4*, 423-426.
7. Koli, P. B., Kapadnis, K. H., Deshpande, U. G.: Nanocrystalline-modified nickel ferrite films: an effective sensor for industrial and environmental gas pollutant detection. *J. Nanostruct. Chem.*, **2019**, *9*, 95-110.
8. Koli, P. B., Kapadnis, K. H., Deshpande, U. G., More, P. B., Tupe, U. J.: Sol-Gel Fabricated Transition Metal Cr^{3+}, Co^{2+} Doped Lanthanum Ferric Oxide (LFO-$LaFeO_3$) Thin Film Sensors for the Detection of Toxic, Flammable Gases: A Comparative Study. *Mater. Sci. Res. India.,* **2020**, *17*, 70-83.
9. Wang, Y., Li, H., He, P., Hosono, E. and Zhou, H.: Nano active materials for lithium-ion batteries. *Nanoscale.*, **2010**, *2*, 1294-1305.
10. Ding, K., Kirchartz, T., Bittkau, K., Lambertz, A., Smirnov, V., Hüpkes, J. Rau, U.: Photovoltaics: Nanoengineered Materials and Their Functionality in Solar Cells. *Nanotechnol. Energy Sustainability.,* **2017**, *5*, 181-206.
11. Patil, M. R., Shrivastava, V. S.: Adsorptive removal of methylene blue from aqueous solution by polyaniline-nickel ferrite nanocomposite: a kinetic approach. *Desalin. Water Treat.*, **2016**, *57*, 5879-5887.
12. Patil, M. R., Khairnar, S. D., Shrivastava, V. S.: Synthesis, characterisation of polyaniline–Fe3O4 magnetic nanocomposite and its application for removal of an acid violet 19 dye. *Appl. Nanosci.*, **2016**, *6*, 495-502.
13. Adole, V. A., Pawar, T. B., Koli, P. B., Jagdale, B. S.: Exploration of catalytic performance of nano-La2O3 as an efficient catalyst for dihydropyrimidinone/thione synthesis and gas sensing. *J. Nanostruct. Chem.*, **2019**, *9*, 61-76.
14. Ahmadi, M.H., Ghazvini, M., Alhuyi Nazari, M., Ahmadi, M.A., Pourfayaz, F., Lorenzini, G., Ming, T.: Renewable energy harvesting with the application of nanotechnology: A review. *Int. J. Energy Res.*, **2019**, *43*, 1387-1410.
15. Abdalla, A.M., Hossain, S., Azad, A.T., Petra, P.M.I., Begum, F., Eriksson, S.G. Azad, A.K.: Nanomaterials for solid oxide fuel cells: a review. *Renewable Sustainable Energy Rev.*, **2018**, *82*, 353-368.
16. Ansari, M. I., Julka, S.: Thakur, D. G.: Enhancement of surface properties with influence of bath pH on electroless Ni-P-ZnO/Al_2O_3 nano-composite deposits for defence applications. *J. Mol. Liq.*, **2017**, *247*, 22-33

17. Dasgupta, N., Ranjan, S., Ramalingam, C.: Applications of nanotechnology in agriculture and water quality management. *Environ. Chem. Lett.*, **2017**, *15*, 591-605.
18. Singh, R., Nalwa, H. S.: Medical applications of nanoparticles in biological imaging, cell labeling, antimicrobial agents, and anticancer nanodrugs. *J. Biomed. Nanotechnol.*, **2011**, *7*, 489-503.
19. Robles-García, M.A.; Rodríguez-Félix, F.; Márquez-Ríos, E.; Aguilar, J. A.; Barrera-Rodríguez, A.; Aguilar, J.; Ruiz-Cruz, S. Del-Toro-Sánchez, C.L.; Applications of nanotechnology in the agriculture, food and pharmaceuticals. *J. Biomed. Nanotechnol.*, **2016**, *16*, 8188-8207.
20. Kim, J., Junkin, M., Kim, D.H., Kwon, S., Shin, Y.S., Wong, P.K. Gale, B.K.: Applications, techniques, and microfluidic interfacing for nanoscale biosensing. *Microfluid. Nanofluid.*, **2009**, *7*, 149-167.
21. Kung, H. H., Kung, M. C.: Nanotechnology: applications and potentials for heterogeneous catalysis. *Catal. Today.*, **2004**, *97*, 219-224.
22. Qu, X.; Alvarez, P. J.; Li, Q.: Applications of nanotechnology in water and wastewater treatment. *Water Res.*, **2013**, *47*, 3931-3946.
23. Koli, P. B.; Kapadnis, K. H.; Deshpande, U. G.; Transition metal decorated Ferrosoferric oxide (Fe_3O_4): An expeditious catalyst for photodegradation of Carbol Fuchsin in environmental remediation. *J. Environ. Chem. Eng.*, **2019**, *7*, 103373.
24. Koli, P. B.; Kapadnis, K. H.; Deshpande, U. G.; Patil, M. R.: Fabrication and characterization of pure and modified Co_3O_4 nanocatalyst and their application for photocatalytic degradation of eosine blue dye: a comparative study. *J. Nanostruct. Chem.*, **2018**, *8*, 453-463.
25. Linh, P.H.; Manh, D.H.; Lam, T.D.; Hong, L.V.; Phuc, N.; Tuan, N.; Ngoc, N. Tuan, V.: Magnetic nanoparticles: study of magnetic heating and adsorption/desorption for biomedical and environmental applications. *Int. J. Nanotechnol.*, **2011**, *8*, 399-413.
26. Seidel, J.: Nanoelectronics based on topological structures Nat. *Mater.*, **2019**, *18*, 188-190.
27. Shinde, V.S.; Kapadnis, K.H.; Sawant, C.P.; Koli, P.B.; Patil, R.P.: Screen Print Fabricated In3+ Decorated Perovskite Lanthanum Chromium Oxide ($LaCrO_3$) Thick Film Sensors for Selective Detection of Volatile Petrol Vapors. *J. Inorg. Organomet. Polym. Mater.*, **2020**, *2,* 1-15.
28. D'amato, G., Environmental urban factors (air pollution and allergens) and the rising trends in allergic respiratory diseases. *Allergy.*, **2002**, *57*, 30-33.
29. Calderón-Garcidueñas, L.; Leray, E.; Heydarpour, P.; Torres-Jardón, R. Reis, J.: Air pollution, a rising environmental risk factor for cognition, neuroinflammation and neurodegeneration: the clinical impact on children and beyond. *Rev. Neurol.*, **2016**, *172*, 69-80.
30. Patella, V.; Florio, G.; Magliacane, D.; Giuliano, A., Crivellaro, M.A.; Di Bartolomeo, D.; Genovese, A.; Palmieri, M.; Postiglione, A.; Ridolo, E. Scaletti, C.: Urban air pollution and climate change: "The Decalogue: Allergy Safe Tree" for allergic and respiratory diseases care. *Clin. Mol. Allergy.*, **2018**, *16*, 1-11.
31. Adole, V.A.; Pawar, T.B.; Jagdale, B.S.: Aqua-mediated rapid and benign synthesis of 1,2,6,7–tetrahydro–8H–indeno[5,4,b] furan–8–one–appended novel 2–arylidene indanones of pharmacological interest at ambient temperature. *J. Chin. Chem. Soc.,* **2020**, *67*, 306-315.
32. Adole, V.A.; Jagdale, B.S.; Pawar, T.B.; Sagane, A.A.: Ultrasound promoted stereoselective synthesis of 2,3-dihydrobenzofuran appended chalcones at ambient temperature. S. *Afr. J. Chem.*, **2019**, *73*, 35-43.
33. Adole, V.A.; Waghchaure, R.H.; Pathade, S.S.; Patil, M.R.; Pawar, T.B.; Jagdale, B.S.: Solvent-free grindstone synthesis of four new (E)-7-(arylidene)-indanones and their structural, spectroscopic and quantum chemical study: a comprehensive theoretical and experimental exploration. *Mol. Simul.*, **2019**, *46*, 1045-1054.
34. Mihailidou, E. K.; Antoniadis, K. D.; Assael, M. J.: The 319 major industrial accidents since 1917. *Int. J. Chem. Eng.*, **2012**, *4*, 529-540.
35. Zhu, L.; Zeng, W.: Room-temperature gas sensing of ZnO-based gas sensor: A review. Sens. *Actuators*, B., **2017**, *267*, 242-261.
36. Dhawale, D. S.; Gujar, T. P.; Lokhande, C. D.: TiO_2 nanorods decorated with Pd nanoparticles for enhanced liquefied petroleum gas sensing performance. *Anal. Chem.*, **2017**, *89*, 8531-8537.

37. Umar, A., Alshahrani, A.A., Algarni, H. Kumar, R.: CuO nanosheets as potential scaffolds for gas sensing applications. Sens. *Actuators*, B., **2017**, *250*, 24-31.
38. Li, Z.; Li, H.; Wu, Z.; Wang, M.; Luo, J.; Torun, H.; Hu, P.; Yang, C.; Grundmann, M.; Liu, X. Fu, Y.: Advances in designs and mechanisms of semiconducting metal oxide nanostructures for high-precision gas sensors operated at room temperature. *Mater. Horiz.*, **2019**, *6*, 470-506.
39. Balasubramani, V.; Chandraleka, S.; Rao, T.S.; Sasikumar, R.; Kuppusamy, M.R. Sridhar, T.M.: Recent Advances in Electrochemical Impedance Spectroscopy Based Toxic Gas Sensors Using Semiconducting Metal Oxides. *J. Electrochem. Soc.*, **2020**, *167*, 37572.
40. Song, Y.G.; Kim, G.S.; Ju, B.K. Kang, C.Y.: Design of Semiconducting Gas Sensors for Room-Temperature Operation. *J. Sens. Technol.*, **2020**, *29*, 1-6.
41. Devi, P. G.; Velu, A. S.; Synthesis, structural and optical properties of pure ZnO and Co doped ZnO nanoparticles prepared by the co-precipitation method. *J. Theor. Appl. Phys.*, **2016**, *10*, 233-240.
42. Hasnidawani, J.N.; Azlina, H.N.; Norita, H.; Bonnia, N.N.; Ratim, S. Ali, E.S.: Synthesis of ZnO nanostructures using sol-gel method. *Procedia Chem.*, **2016**, *19*, 211-216.
43. Kulandaisamy, A.J.; Reddy, J.R.; Srinivasan, P.; Babu, K.J.; Mani, G.K.; Shankar, P. Rayappan, J.B.B.: Room temperature ammonia sensing properties of ZnO thin films grown by spray pyrolysis: Effect of Mg doping. *J. Alloys Compd.*, **2016**, *688*, 422-429.
44. Iwan, S.; Zhao, J.L.; Tan, S.T. Sun, X.W.: Enhancement of UV photoluminescence in ZnO tubes grown by metal organic chemical vapour deposition (MOCVD). *Vacuum.,* **2018**, *155*, 408-411.
45. Das, B.K.; Das, T.; Parashar, K.; Thirumurugan, A. Parashar, S.K.S.: Structural, bandgap tuning and electrical properties of Cu doped ZnO nanoparticles synthesized by mechanical alloying. *J. Mater. Sci.: Mater. Electron.*, **2017**, *28*, 15127-15134.
46. Jamshidi, M.; Ghaedi, M.; Dashtian, K.; Hajati, S. Bazrafshan, A.A.: Sonochemical assisted hydrothermal synthesis of ZnO: Cr nanoparticles loaded activated carbon for simultaneous ultrasound-assisted adsorption of ternary toxic organic dye: derivative spectrophotometric, optimization, kinetic and isotherm study. Ultrason. *Sonochem.*, **2016,** *32*, 119-131.
47. Alammar, A. T.; Mudring, V.: Facile ultrasound-assisted synthesis of ZnO nanorods in an ionic liquid. *Mater. Lett.*, **2009**, *63*, 732-735.
48. Kumar, V.; Gohain, M.; Som, S.; Kumar, V.; Bezuindenhoudt, B.C.B., Swart, H.C.: Microwave assisted synthesis of ZnO nanoparticles for lighting and dye removal application. *Phys.* B., **2016**, *480*, 36-41.
49. Bhati, V.S.; Hojamberdiev, M.; Kumar, M.: Enhanced sensing performance of ZnO nanostructures-based gas sensors: *A review. Energy Rep.*, **2020**, *6*, 46-62.
50. Galatsis, K.; Li, Y.X.; Wlodarski, W.; Comini, E.; Sberveglieri, G.; Cantalini, C.; Santucci, S.; Passacantando, M.: Comparison of single and binary oxide MoO_3, TiO_2 and WO_3 sol–gel gas sensors. *Sens. Actuators*, B., **2002**, *83*, 276-280.
51. Shinde, V.S.; Sawant, C.P.; Kapadnis, K.H.: Modified Sn-doped $LaCrO_3$ nanostructures: focus on their characterization and applications as ethanol sensor at a lower temperature. *J. Nanostruct. Chem.*, **2019**, *9*, 231-245.
52. Alqarni, S.A.; Hussein, M.A.; Ganash, A.A.; Khan, A.: Composite Material–Based Conducting Polymers for Electrochemical Sensor Applications: a Mini Review. *Bio Nano Science.,* **2020**, *1*, 1-14.
53. Justino, C.I.; Gomes, A.R.; Freitas, A.C.; Duarte, A.C.; Rocha-Santos, T.A.: Graphene based sensors and biosensors. TrAC, *Trends Anal. Chem.*, **2017**, *91*, 53-66.
54. Kiani, M.; Bagherzadeh, M.; Meghdadi, S., Rabiee, N.; Abbasi, A., Schenk-Joß, K., Tahriri, M.; Tayebi, L.; Webster, T.J.: Development of a novel carboxamide-based off–on switch fluorescence sensor: Hg^{2+}, Zn^{2+} and Cd^{2+}. *New J. Chem.*, **2020**, *44*, 11841-11852.
55. Wang, Y.; Kim, S. H.; Feng, L.: Highly luminescent N, S-Co-doped carbon dots and their direct use as mercury (II) sensor. *Anal. Chim. Acta.*, **2015**, *890*, 134-142.
56. Shen, J.Y.; Zhang, L.; Ren, J.; Wang, J.C.; Yao, H.C.; Li, Z.J.: Highly enhanced acetone sensing performance of porous C-doped WO_3 hollow spheres by carbon spheres as templates. Sens. *Actuators*, B., **2017**, *239*, 597-607.

57. Qu, J.; Ge, Y.; Zu, B.; Li, Y.; Dou, X.: Transition, Metal, Doped p, Type ZnO Nanoparticle, Based Sensory Array for Instant Discrimination of Explosive Vapors. *Small.,* **2016**, *12*, 1369-1377.
58. Alam, M.M.; Asiri, A.M.; Uddin, M.T.; Islam, M.A.; Awual, M.R.; Rahman, M.M.: Detection of uric acid based on doped ZnO/Ag_2O/Co_3O_4 nanoparticle loaded glassy carbon electrode. *New J. Chem.*, **2019**, *43*, 8651-8659.
59. Celiesiute, R.; Ramanaviciene, A.; Gicevicius, M.; Ramanavicius, A.: Electrochromic sensors based on conducting polymers, metal oxides, and coordination complexes. *Crit. Rev. Anal. Chem.*, **2019**, *49*, 195-208.
60. Ueda, K.; Tabata, H.; Kawai, T.: Magnetic and electric properties of transition-metal-doped ZnO films. *Appl. Phys. Lett.*, **2001**, *79*, 988-990.
61. Ferhat, M.; Zaoui, A.; Ahuja, R.: Magnetism and band gap narrowing in Cu-doped ZnO. *Appl. Phys. Lett.*, **2009**, *94*, 142502.
62. Saleh, R.; Djaja, N. F.: Transition-metal-doped ZnO nanoparticles: synthesis, characterization and photocatalytic activity under UV light. *Spectrochim. Acta*, Part A., **2014**, *130*, 581-590.
63. Hasegawa, H.; Kobayashi, K.; Takahashi, Y.; Harada, J. Inabe, T.: Effective band gap tuning by foreign metal doping in hybrid tin iodide perovskites. *J. Mater. Chem.*, **2017**, *5*(16), 4048-4052.
64. S Shinde, S.G.; Patil, M.P.; Kim, G.D.; Shrivastava, V.S.: Multi-doped ZnO Photocatalyst for Solar Induced Degradation of Indigo Carmine Dye and as an Antimicrobial Agent. *J. Inorg. Organomet. Polym. Mater.*, **2019**, *10,* 1-12.
65. Ganesh, V.; Yahia, I.S.; AlFaify, S.; Shkir, M.: Sn-doped ZnO nanocrystalline thin films with enhanced linear and nonlinear optical properties for optoelectronic applications. *J. Phys. Chem. Solids.,* **2017**, *100*, 115-125.
66. Sharma, D.; Jha, R.; Transition metal (Co, Mn) co-doped ZnO nanoparticles: effect on structural and optical properties. *Journal of Alloys and Compounds.*, **2017**, *698*, 532-538.
67. Chapelle, A.; Oudrhiri-Hassani, F.; Presmanes, L.; Barnabé, A.; Tailhades, P.: CO_2 sensing properties of semiconducting copper oxide and spinel ferrite nanocomposite thin film. *Appl. Surf. Sci.*, **2010**, *256*, 4715-4719.
68. Sonker, R. K.; Yadav, B. C.: Low temperature study of nanostructured Fe_2O_3 thin films as NO_2 sensor. *Mater. Today*. *Proc.*, **2016**, *3*, 2315-2320.
69. Iwata, T.; Matsuda, K.; Takahashi, K.; Sawada, K.: CO_2 sensing characteristics of a La_2O_3/SnO_2 stacked structure with micromachined hotplates. *Sensors.,* **2017**, *17*, 2156.
70. Hong, H.S.; Dai Lam, T.; Trung, T.; Van Hieu, N.: Selective detection of carbon dioxide using LaOCl-functionalized SnO_2 nanowires for air-quality monitoring. *Talanta.,* **2012**, *88*, 152-159.
71. Manasa, M.V.; Devi, G.S.; Reddy, P.P.: Selective CO_2 Gas Sensor via Noble Metal Functionalized Nano MoO_3: NiO. *Int. J. New Technol. Sci. Eng.*, **2018**, *5*, 43-53.
72. Tanuma, R.; Sugiyama, M.: Polycrystalline SnO_2 Visible, Light, Transparent CO_2 Sensor Integrated with NiO/ZnO Solar Cell for Self, Powered Devices. Phys. *Status Solidi* A., **2019**, *216*, 1800749-1800753.